Gut and Liver
https://doi.org/10.5009/gnl210195
pISSN 1976-2283 eISSN 2005-1212

Original Article

circ-LDLRAD3 Knockdown Reduces Cisplatin Chemoresistance and Inhibits the Development of Gastric Cancer with Cisplatin Resistance through miR-588 Enrichment-Mediated SOX5 Inhibition

Qianping Liang, Feifei Chu, Lei Zhang, Yuanyuan Jiang, Lu Li, and Huili Wu

Department of Gastroenterology, Zhengzhou Central Hospital Affiliated to Zhengzhou University, Zhengzhou, China

Article Info
Received June 8, 2021
Revised December 2, 2021
Accepted December 21, 2021
Published online August 17, 2022

Corresponding Author
Huili Wu
ORCID https://orcid.org/0000-0002-9678-4596
E-mail wuhuili660912@126.com

Background/Aims: Chemoresistance is a common event after cancer chemotherapy, which is associated with the deregulation of circular RNAs (circRNAs). The objective of this study was to clarify the role of circ-LDLRAD3 in cisplatin (DDP)-resistant gastric cancer (GC).

Methods: The expression of circ-LDLRAD3, miR-588, and SRY-box transcription factor 5 (SOX5) mRNA was detected by quantitative real-time polymerase chain reaction. Cell viability and the half maximal inhibitory concentration (IC_{50}) value were measured by CCK8 assay. Cell proliferation was assessed by colony formation and EdU assays. Cell apoptosis and cell invasion were assessed by flow cytometry assay and transwell assay, respectively. The expression of SOX5 protein was detected by Western blotting. A xenograft model was established to verify the role of circ-LDLRAD3 *in vivo*. Exosomes were isolated by differential centrifugation and identified by transmission electron microscopy and the expression of exosome-related proteins.

Results: circ-LDLRAD3 was overexpressed in DDP-resistant GC tissues and cells. circ-LDLRAD3 knockdown decreased the IC_{50} of DDP-resistant cells and suppressed cell proliferation, survival and invasion. miR-588 was a target of circ-LDLRAD3, and miR-588 inhibition attenuated the inhibition of DDP resistance, proliferation, survival and invasion in DDP-resistant GC cells caused by circ-LDLRAD3 knockdown. SOX5 was a target of miR-588, and the inhibition of the DDP resistance, proliferation, survival and invasion of DDP-resistant GC cells by miR-588 restoration was largely rescued SOX5 overexpression. circ-LDLRAD3 knockdown inhibited DDP resistance and tumor growth *in vivo*. circ-LDLRAD3 was overexpressed in exosomes isolated from DDP-resistant GC cells.

Conclusions: circ-LDLRAD3 knockdown reduced DDP resistance and blocked the malignant development of DDP-resistant GC by modulating the miR-588/SOX5 pathway. **(Gut Liver 2023;17:389-403)**

Key Words: circ-LDLRAD3; miR-588; SOX5; Cisplatin; Stomach neoplasms

INTRODUCTION

Gastric cancer (GC), the third most common cause of cancer-related death in the world, is a major health problem.[1] Radical gastrectomy is the main treatment for early GC. However, many GC patients cannot be diagnosed early due to the invisibility of the disease and the lack of appropriate early detection technology.[2] For these patients, systemic chemotherapy, such as cisplatin (DDP), is the main mainstay of treatment.[3] Unfortunately, in advanced cancer patients, inherent or acquired drug resistance leads to more than 90% of unsuccessful treatments.[4] A better understanding of the drivers associated with chemoresistance may ultimately lead to the optimization of treatment strategies for GC patients.

Circular RNAs (circRNAs) are famous for their continuous loop-closed structures. Recently, circRNAs are shown to be extensively expressed in cancer tissues, serum and cells by RNA sequencing technology.[5] Unlike linear molecules, circRNAs are stable and resistant RNase R diges-

tion, which makes them promising biomarkers in cancer therapy.[6] Emerging studies demonstrate that circRNAs are involved in cancer initiation, development, radioresistance and chemoresistance.[7] For instance, circ-AKT3 overexpression strengthened DDP resistance in GC and thus inhibited GC cell apoptosis after DDP treatment.[8] Previous studies provided circRNA expression profiles by performing RNA sequencing, which was uploaded on the public database GEO. For example, we analyzed the GEO dataset (GSE93541) and obtained numerous differently expressed circRNAs in plasma samples from GC patients. Hsa_circ_0006988 (circ-LDLRAD3), was shown to be expressed in plasma from GC patients with a high level, hinting that circ-LDLRAD3 might be involved in GC development. Nevertheless, the role of circ-LDLRAD3 in GC was rarely explored and needed further investigation.

MicroRNAs (miRNAs) have been extensively studied in human cancer, widely involving in diagnosis, progression and immune surveillance.[9] Interestingly, the expression of miRNAs can be sequestered by certain circRNAs through "sponge" effects,[10] which provides a new idea to understand the action mechanism of circRNAs. Besides, miRNAs regulate gene expression by targeting binding sites of the 3' untranslated region (3'UTR) of target genes.[11] Based on these opinions, bioinformatics tools present that there are binding sites of miR-588 on circ-LDLRAD3 and SRY-box transcription factor 5 (SOX5) 3'UTR. MiR-588 was previously shown to be a tumor suppressor in GC,[12] while SOX5 promoted the malignant development in GC.[13] The data exposed that miR-588 and SOX5 were implicated in GC progression. However, it was not clear whether the involvement of miR-588 and SOX5 in GC was associated with circ-LDLRAD3 regulation.

Here, we mainly disclosed the role of circ-LDLRAD3 in DDP chemoresistance, cell growth, survival and invasion in DDP-resistant GC cells *in vitro*. Besides, we identified the binding relationship between miR-588 and circ-LDLRAD3 or SOX5, and demonstrated a novel mechanism to understand the effects of circ-LDLRAD3 in DDP-resistant GC. Our study provided a reference for understanding the pathogenesis of GC with DDP resistance.

MATERIALS AND METHODS

1. Public database

circRNA expression profile was obtained from GEO database (GSE93541: https://www.ncbi.nlm.nih.gov/geo/query/acc.cgi?acc=GSE93541). Bioinformatics tool (starBase: http://starbase.sysu.edu.cn/) for target prediction was applied in this study.

2. Clinical samples

A total of 46 tumor tissues and paired normal tissues that were preserved at Zhengzhou Central Hospital Affiliated to Zhengzhou University were used in this study. These patients received DDP treatment and classified into two groups according to therapeutic outcomes, including DDP-resistant group (n=27; non-response or deterioration) and DDP-sensitive group (n=19; partial/complete remission). All patients and their families approved the experiment and signed written informed consent. Tissue samples were surgically excised from body after DDP chemotherapy. Relationship between circ-LDLRAD3 expression and clinicopathologic features of GC patients was summarized in Table 1. This study was approved by the Ethics Committee of Zhengzhou Central Hospital Affiliated to Zhengzhou University (approval number: 20210318).

3. Cell lines

GC cells (NCI-N87, HGC-27, and AGS) were obtained from Bena (Beijing, China) and cultured in RPMI-1640 (Gibco, Grand Island, NY, USA) or F-12K medium (Gibco) containing 10% fetal bovine serum (Gibco) as appropriate. Non-cancer cells (GES-1) were also purchased from Bena and cultured in RPMI-1640 medium containing 10% fetal bovine serum.

DDP-resistant GC cells were established by treating

Table 1. Relationship between circ-LDLRAD3 Expression and Clinicopathologic Features of Gastric Cancer Patients

Characteristics	No.	circ-LDLRAD3		p-value*
		Low (n=23)	High (n=23)	
Total	46			
Sex				0.7631
Female	28	13	15	
Male	18	10	8	
Age				0.7575
≤60 yr	16	9	7	
>60 yr	30	14	16	
TNM grade				0.0331
I+II	18	13	5	
III+IV	28	10	18	
Lymph node metastasis				0.0023
Positive	27	8	19	
Negative	19	15	4	
Tumor size				0.0018
≤5 cm	17	14	3	
>5 cm	29	9	20	
Histologic grade				0.0003
Intestinal type	21	17	4	
Diffuse type	25	6	19	

TNM, tumor-node-metastasis.
*Chi-square test: statistically significant, p<0.05.

HGC-27 and AGS cells with gradually increasing concentrations of DDP (0.5–10 μg/mL; Sigma-Aldrich, St. Louis, MO, USA) for over 6 months, to establish DDP-resistant HGC-27 cell line (HGC-27/CDDP) and CDDP-resistant AGS (AGS/CDDP) cell line.

4. Quantitative real-time polymerase chain reaction

After RNA isolation using Trizol reagent (Takara, Dalian, China), cDNA was synthesized using a PrimeScript RT Reagent Kit (Takara) or miRcute Plus miRNA First-Strand cDNA Kit (Tiangen, Beijing, China). Then, SuperReal PreMix Color (SYBR Green; Tiangen) was used for quantitative real-time polymerase chain reaction (qPCR) amplification. Relative expression was processed using the $2^{-\Delta\Delta Ct}$ method, with GAPDH or U6 as an internal inference. The sequences of primers were shown as below:

Circ-LDLRAD3, F: 5'-GACCAGAGAACCCGGCAG-3' and R: 5'-CAGCGTCATGAGGTTGTTCC-3'; LDLRAD3, F: 5'-GCCTGACTGCTTCGACAAGA-3' and R: 5'-AATGATGCAATGGATGCCGC-3'; miR-588, F: 5'-GCGTTGGCCACAATGGGT-3' and R: 5'-AGTGCAGGGTCCGAGGTATT-3'; SOX5, F: 5'-CGTCCTCCATATAACCGAGC-3' and R: 5'-TCATAGGTTCCATTCTGCCG-3'; U6, F: 5'-CTCGCTTCGGCAGCACA-3' and R: 5'-AACGCTTCACGAATTTGCGT-3'; GAPDH, F: 5'-GATGCTGGCGCTGAGTACG-3' and R: 5'-GCTAAGCAGTTGGTGGTGC-3'.

5. RNase R treatment

Total RNA isolated from cells was exposed to RNase R (3 U/μg; Epicentre, Madison, WI, USA) and then used for qPCR analysis.

6. Cell transfection

The assembled siRNA targeting circ-LDLRAD3 (si-circ-LDLRAD3) and its negative control (si-NC), circ-LDLRAD3 overexpression vector (circ-LDLRAD3) and pCD5-ciR blank vector (pCD5-ciR) were all obtained from Geneseed (Shanghai, China). miR-588 mimic (miR-588), miR-588 inhibitor (anti-miR-588), and their matched control (miR-NC and anti-miR-NC) were purchased from Ribobio (Guangzhou, China). SOX5 overexpression vector (SOX5) and matched blank vector (pcDNA) were provided by Genepharma (Shanghai, China). Lipofectamine 3000 reagent (Invitrogen, Carlsbad, CA, USA) was used for cell transfection.

7. CCK-8 assay

Cells were incubated in 96-well plates (3×10^3 cell/well) and continued to culture for 24 hours. CCK-8 reagent (Beyotime, Shanghai, China) was used to incubate cells for 2 hours. The optical density value of cells was measured at 450 nm using a spectrophotometer (Bio-Rad, Hercules, CA, USA). AGS/DDP and HGC-27/DDP cells were treated with different doses of DDP. Cell viability was next checked after 24 hours, and half maximal inhibitory concentration (IC_{50}) of DDP in these cells was obtained via cell viability curve.

8. Colony formation assay

Cells were incubated in 6-well plates (200 cells/well) for 2 weeks to induce colony formation. Cell colonies were fixed and stained with crystal violet (Beyotime). The formation of colonies was observed by a light microscope (Leica, Wetzlar, Germany).

9. EdU assay

Cell proliferation was assessed by EdU assay using Cell-Light EdU Apollo567 in Vitro Kit (Ribobio) in accordance with the protocol. Images were taken using a fluorescence microscope (Leica).

10. Flow cytometry assay

Cell apoptosis was checked using an Annexin V-FITC and propidium iodide Apoptosis Detection Kit (KeyGEN Biotech, Nanjing, China). In brief, AGS/DDP and HGC-27/DDP cells were suspended in Annexin V-FITC binding buffer. Afterwards, Annexin V/FITC and propidium iodide solution were used to stain cells. FACScan flow cytometry (BD Biosciences, San Jose, CA, USA) was used for flow cytometry assay.

11. Transwell assay

RPMI-1640 medium or F-12K medium cultured with HGC-27/DDP cells or AGS/DDP cells was supplemented to the upper transwell chambers (Corning Incorporated, Corning, NY, USA) coated with Matrigel (BD Biosciences), and RPMI-1640 medium or F-12K medium containing 10% fetal bovine serum was added to the lower chamber. After incubation for 24 hours, the invaded cells were fixed with paraformaldehyde, stained with 0.5% crystal violet and observed by a microscope (Leica).

12. Western blot

Western blot assay was conducted as previously mentioned.[14] The primary antibodies, including anti-cyclin D1 (ab16663), anti-MMP9 (ab137867), anti-SOX5 (ab94396), and the secondary (ab205718) were all purchased from Abcam (Cambridge, MA, USA).

13. Dual-luciferase reporter assay

According to the wild-type (WT) binding sites of miR-588 on circ-LDLRAD3 and SOX5 3'UTR, the mutant (MUT) sequences of circ-LDLRAD3 and SOX5 were designed. By using pmirGLO plasmid (Promega, Madison,

WI, USA), WT-circ-LDLRAD3, MUT-circ-LDLRAD3, WT-SOX5 3'UTR, and MUT-SOX5 3'UTR reporter plasmids were constructed. These reporter plasmids were separately transfected with miR-588 or miR-NC into AGS/DDP and HGC-27/DDP cells, incubating for 48 hours. Luciferase activity in these transfected cells was examined using the Luciferase Reporter assay system (Promega).

14. Xenograft model

Animal study was permitted by the Animal Care and Use Committee of Zhengzhou Central Hospital Affiliated to Zhengzhou University (approval number: 20210318). The experimental mice (BALB/c, female, n=24) were purchased from Vitalriver (Beijing, China) and divided into four groups: sh-NC+phosphate-buffered saline (PBS), sh-NC+DDP, sh-circ-LDLRAD3+PBS, and sh-circ-LDLRAD3+DDP. The lentivirus suspensions of sh-circ-LDLRAD3 or sh-NC were provided by Geneseed. AGS/DDP cells were infected with lentivirus-packaged sh-circ-LDLRAD3 or sh-NC and then implanted into nude mice by subcutaneous injection. The

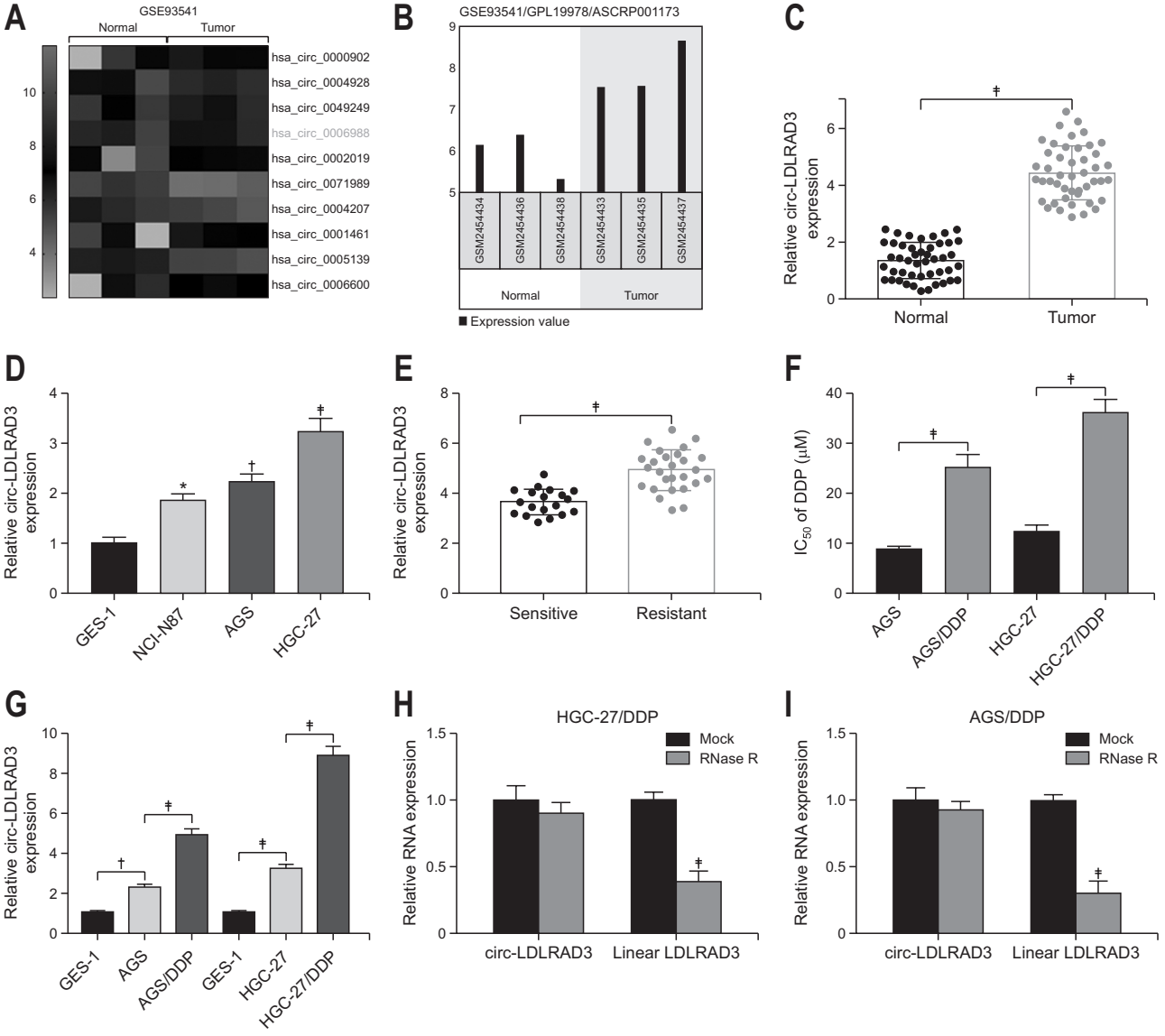

Fig. 1. circ-LDLRAD3 is overexpressed in DDP-resistant GC tissues and cells. (A, B) The public database (GSE93541) provided differently expressed circRNAs in tumor tissues of GC, and circ-LDLRAD3 was notably upregulated in tumor tissues. (C) The expression of circ-LDLRAD3 in our clinical tumor tissues and normal tissues was detected by qPCR. (D) The expression of circ-LDLRAD3 in GES-1, NCI-N87, AGS and HGC-27 cells was detected by qPCR. (E) The expression of circ-LDLRAD3 in DDP-resistant/sensitive tumor tissues was detected by qPCR. (F) The IC_{50} of AGS/DDP, HGC-27/DDP and their parental cells was detected. (G) The expression of circ-LDLRAD3 in AGS/DDP, HGC-27/DDP and their parental cells was detected by qPCR. (H, I) The stability of circ-LDLRAD3 was assessed after RNase R treatment.
circ-LDLRAD3, hsa_circ_0006988; DDP, cisplatin; GC, gastric cancer; circRNA, circular RNA; qPCR, quantitative real-time polymerase chain reaction; IC_{50}, half maximal inhibitory concentration. *p<0.01, †p<0.001, ‡p<0.0001.

experimental mice were administered with DDP or PBS at a dose of 1.5 mg/kg in each mouse by intratumoral injection. During tumor growth, tumor volume (0.5×length×width^2) was measured every 3 days. At 23 days posttreatment, these mice were sacrificed, and tumor tissues in mice were excised for subsequent assays.

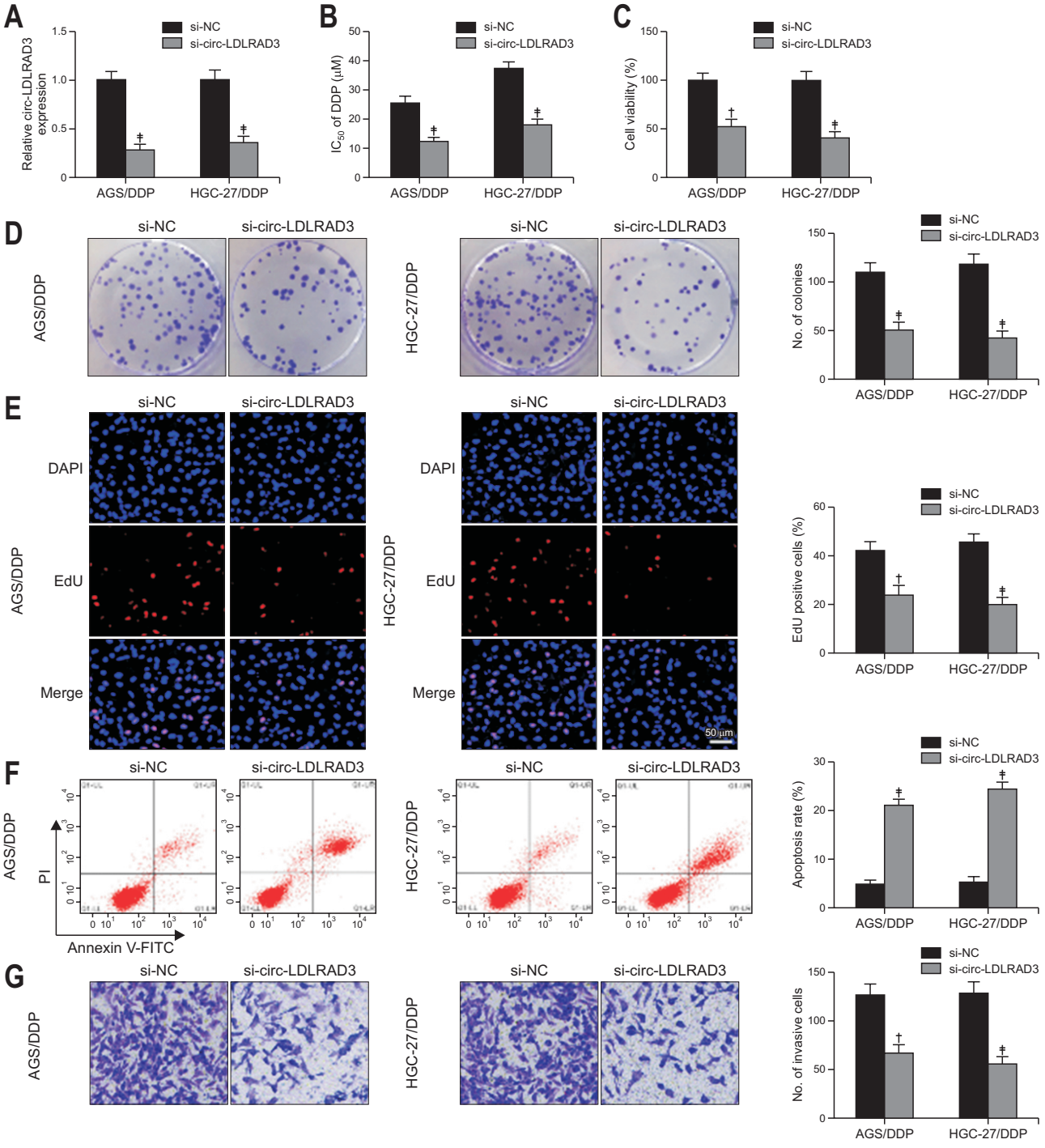

Fig. 2. circ-LDLRAD3 knockdown inhibited DDP resistance of AGS/DDP and HGC-27/DDP cells and blocked cell proliferation, survival and invasion. (A) The efficiency of si-circ-LDLRAD3 was assessed by qPCR. In AGS/DDP and HGC-27/DDP cells, (B) the IC_{50} of DDP, and (C) the cell viability were assessed by CCK-8 assay. (D, E) Cell proliferation was assessed by colony formation assay and EdU assay. (F) Cell apoptosis was monitored by flow cytometry assay. (G) Cell invasion was monitored by Transwell assay. (H, I) The protein levels of cyclin D1 and MMP9 were detected by Western blotting.

Circ-LDLRAD3, hsa_circ_0006988; DDP, cisplatin; NC, negative control; qPCR, quantitative real-time polymerase chain reaction; PI, propidium iodide; IC_{50}, half maximal inhibitory concentration. *p<0.001, †p<0.0001, ‡p<0.0001.

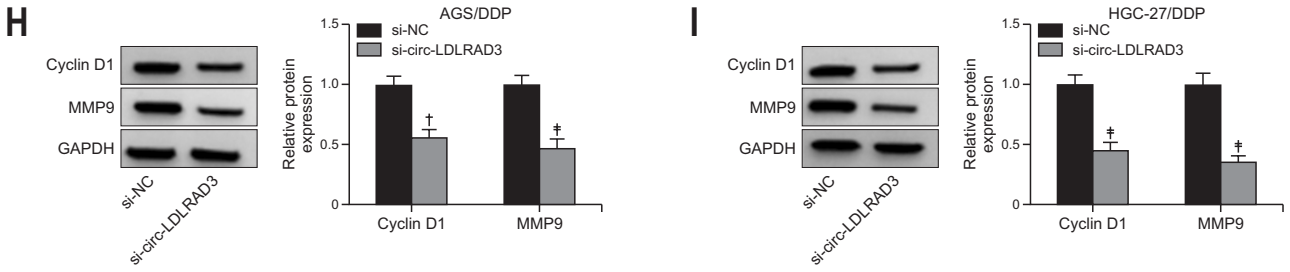

Fig. 2. Continued.

15. Immunohistochemistry (IHC) assay

Tissue sections (6 μm-thick) were prepared, dewaxed, rehydrated and subjected to antigen retrieval. Tissue sections were incubated with the primary antibodies, including anti-SOX5 (K004916P; Solarbio, Beijing, China) and anti-Ki67 (K009725P; Solarbio). Then, tissue sections were incubated with goat-anti rabbit IgG-HRP (SE134; Solarbio). The sections were counterstained using the diaminobenzidine substrate kit (Solarbio) and observed under a light microscope (Leica).

16. Exosomes isolation and identification

Exosomes were isolated from cells using an exoEasy Maxi Kit (QIAGEN, Duesseldorf, Germany) by differential centrifugation.

The morphology of exosomes was identified by transmission electron microscopy. Simply put, the isolated exosomes resuspended in PBS were placed on a chloroform-coated copper grid with 0.125% Formvar and subjected to 1% uranyl acetate staining buffer. Images were observed under a transmission electron microscopy (Hitachi, Tokyo, Japan).

Besides, exosomes were identified by exosome-related markers, including CD63 and CD9, using Western blot. The primary antibodies against CD63 (ab134045; Abcam) and CD9 (ab92726; Abcam) were used here.

17. Statistical analysis

The data from at least three independent experiments were processed by GraphPad Prism 7 software (GraphPad Inc., La Jolla, CA, USA). The difference of data between groups was compared and analyzed by the Student t-test, and the difference of data among multiple groups were analyzed by the analysis of variance, followed by Tukey test. The correlation between two sets was analyzed by the Pearson correlation analysis. Data are shown as the mean±standard deviation. $p<0.05$ was considered to be statistically significant difference.

RESULTS

1. circ-LDLRAD3 was highly expressed in DDP-resistant GC tissues and cells

We processed the data from the public database GEO (GSE93541) and found that hsa_circ_0006988 (circ-LDLRAD3) was one of the upregulated circRNAs in tumor tissues (n=3) compared to normal tissues (n=3) (Fig. 1A and B). In our clinical samples, we confirmed that circ-LDLRAD3 expression was notably increased in tumor tissues (n=46) of GC (Fig. 1C). The expression of circ-LDLRAD3 was also increased in NCI-N87, AGS and HGC-27 cells compared to GES-1 cells (Fig. 1D). Moreover, circ-LDLRAD3 expression was relatively higher in DDP-resistant tumor tissues (n=27) than that in DDP-sensitive tumor tissues (n=19) (Fig. 1E). DDP-resistant AGS and HGC-27 cells were generated, and we found that the IC_{50} of DDP was higher in AGS/DDP and HGC-27/DDP cells than that in AGS and HGC-27 cells (Fig. 1F). Circ-LDLRAD3 expression was also enhanced in AGS/DDP and HGC-27/DDP cells compared with that in AGS and HGC-27 cells (Fig. 1G). In addition, circ-LDLRAD3, relative to linear LDLRAD3, was noticeably resistant to RNase R digestion (Fig. 1H and I). The aberrant upregulation of circ-LDLRAD3 in DDP-resistant GC tissues and cells hinted that circ-LDLRAD3 was involved in the development of chemoresistance in GC.

2. circ-LDLRAD3 knockdown reduced chemoresistance and inhibited the growth and invasion in DDP-resistant GC cells

We reduced the expression level of circ-LDLRAD3 in AGS/DDP and HGC-27/DDP cells by transfecting si-circ-LDLRAD3 (Fig. 2A). We discovered that circ-LDLRAD3 knockdown reduced the IC_{50} of DDP in AGS/DDP and HGC-27/DDP cells (Fig. 2B). Besides, the data from CCK-8 assay, colony formation assay and EdU assay presented that circ-LDLRAD3 knockdown inhibited cell viability, colony formation ability and the number of EdU-positive cells, suggesting that circ-LDLRAD3 knockdown inhibited AGS/DDP and HGC-27/DDP cell growth (Fig. 2C-E). The

data from flow cytometry assay presented that circ-LDLRAD3 knockdown promoted AGS/DDP and HGC-27/DDP cell apoptosis (Fig. 2F). The data from transwell assay presented that circ-LDLRAD3 knockdown suppressed AGS/DDP and HGC-27/DDP cell invasion (Fig. 2G). The expression of cell cycle marker and invasion marker was quantified, and the expression of cyclin D1 and MMP9 was notably decreased in AGS/DDP and HGC-27/DDP cells after circ-LDLRAD3 knockdown (Fig. 2H and I). The data suggested that circ-LDLRAD3 inhibited DDP resistance and cell malignant behaviors in DDP-resistant GC cells.

3. circ-LDLRAD3 targeted miR-588 and suppressed miR-588 expression

The data from bioinformatics database showed that circ-LDLRAD3 is bound to miR-588 through several binding sites (Fig. 3A). The expression of miR-588 was markedly promoted in AGS/DDP and HGC-27/DDP cells transfected with miR-588 (Fig. 3B). Besides, the cotransfection of miR-588 and WT-circ-LDLRAD3 significantly reduced luciferase activity, verifying the binding between miR-588 and circ-LDLRAD3 (Fig. 3C and D). The expression of miR-588 was remarkably decreased in DDP-resistant tumor tissues compared to DDP-sensitive tumor tissues (Fig. 3E), and miR-588 expression was negatively correlated with circ-LDLRAD3 expression in DDP-resistant tumor tissues (Fig. 3F). Likewise, miR-588 expression was decreased in AGS/DDP and HGC-27/DDP cells compared with that in AGS and HGC-27 cells (Fig. 3G). In AGS/DDP and HGC-27/DDP cells transfected with circ-LDLRAD3, the expression of circ-LDLRAD3 was notably increased (Fig. 3H). Moreover, the expression of miR-588 was enhanced in cells after circ-LDLRAD3 knockdown but declined in cells after circ-LDLRAD3 overexpression (Fig. 3I). Overall, miR-588 was a target of circ-LDLRAD3.

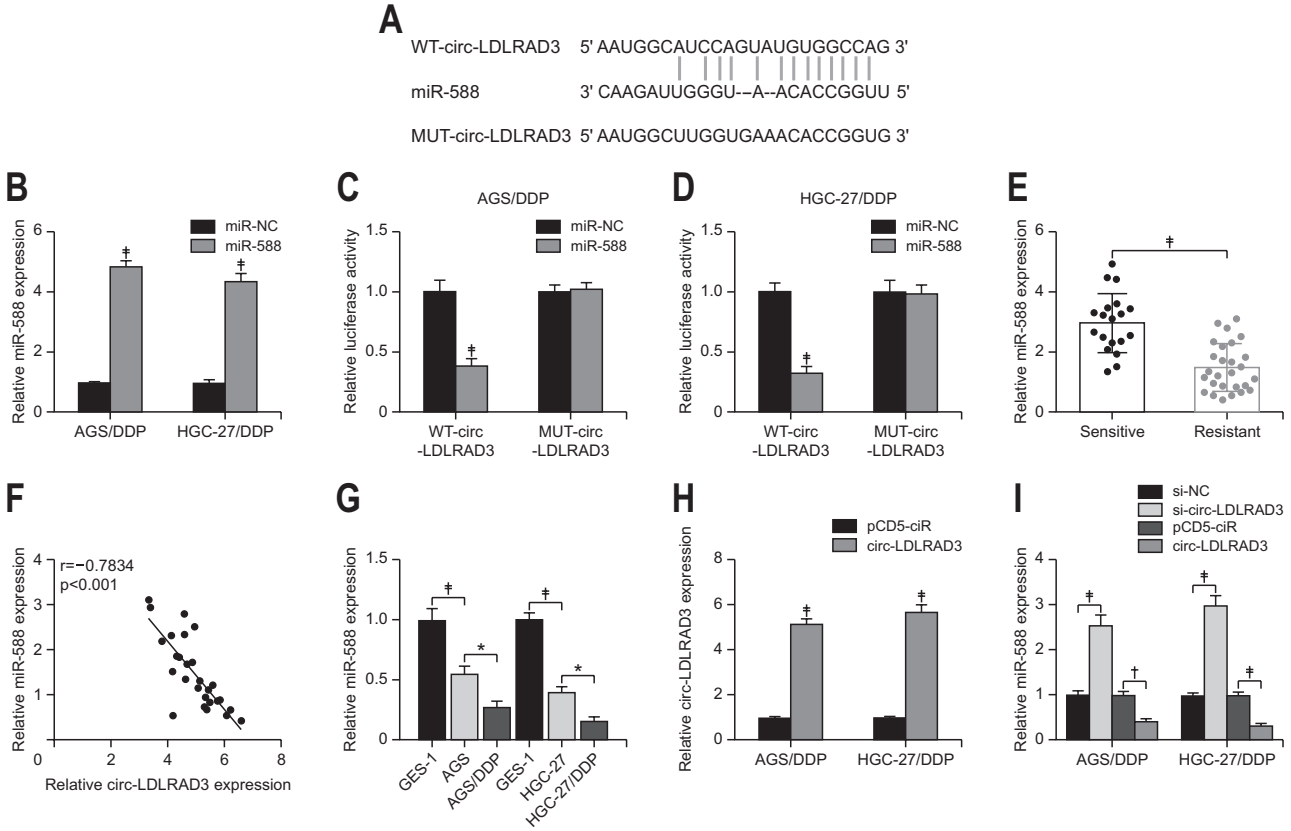

Fig. 3. miR-588 is a target of circ-LDLRAD3. (A) The WT and MUT sequences of circ-LDLRAD3 were shown. (B) The efficiency of miR-588 mimic was assessed by qPCR. (C, D) The binding relationship between miR-588 and circ-LDLRAD3 was verified by dual-luciferase reporter assay. (E) The expression of miR-588 in DDP-resistant/sensitive tumor tissues was detected by qPCR. (F) The linear relationship between miR-588 expression and circ-LDLRAD3 expression in tumor tissues. (G) The expression of miR-588 in AGS/DDP, HGC-27/DDP and their parental cells was detected by qPCR. (H) The efficiency of circ-LDLRAD3 overexpression was assessed by qPCR. (I) The expression of miR-588 in AGS/DDP and HGC-27/DDP cells with circ-LDLRAD3 knockdown or overexpression was detected by qPCR.
WT, wild-type; MUT, mutant; circ-LDLRAD3, hsa_circ_0006988; DDP, cisplatin; NC, negative control; qPCR, quantitative real-time polymerase chain reaction; IC_{50}, half maximal inhibitory concentration. *p<0.01, †p<0.001, ‡p<0.0001.

4. The inhibition of miR-588 reversed the role of circ-LDLRAD3 knockdown

We continued to explore the interactions between circ-LDLRAD3 and miR-588 in AGS/DDP and HGC-27/DDP cells. The expression of miR-588 was markedly declined in AGS/DDP and HGC-27/DDP cells after anti-miR-588 transfection (Fig. 4A). Besides, the expression of miR-588 was markedly enhanced by si-circ-LDLRAD3 but partially repressed by si-circ-LDLRAD3+anti-miR-588 (Fig. 4B). The IC_{50} of DDP in AGS/DDP and HGC-27/DDP cells was weakened by circ-LDLRAD3 knockdown but recovered by miR-588 inhibition (Fig. 4C). The data from CCK-8 assay, colony formation assay and EdU assay indicated that the ability of AGS/DDP and HGC-27/DDP cell proliferation was suppressed by circ-LDLRAD3 knockdown but recovered by miR-588 inhibition (Fig. 4D-F). Circ-LDLRAD3 knockdown-induced cell apoptosis was relieved by miR-588 inhibition (Fig. 4G). The number of invaded cells was decreased in AGS/DDP and HGC-27/DDP cells transfected with si-circ-LDLRAD3 but restored in cells transfected with si-circ-LDLRAD3+anti-miR-588 (Fig. 4H). The protein levels of cyclin D1 and MMP9 in AGS/DDP and HGC-27/DDP cells were repressed by circ-LDLRAD3 knockdown but partially recovered by additional miR-588 inhibition (Fig. 4I and J). Overall, circ-LDLRAD3 inhibited DDP resistance and cell malignant behaviors in DDP-resistant GC cells by increasing miR-588.

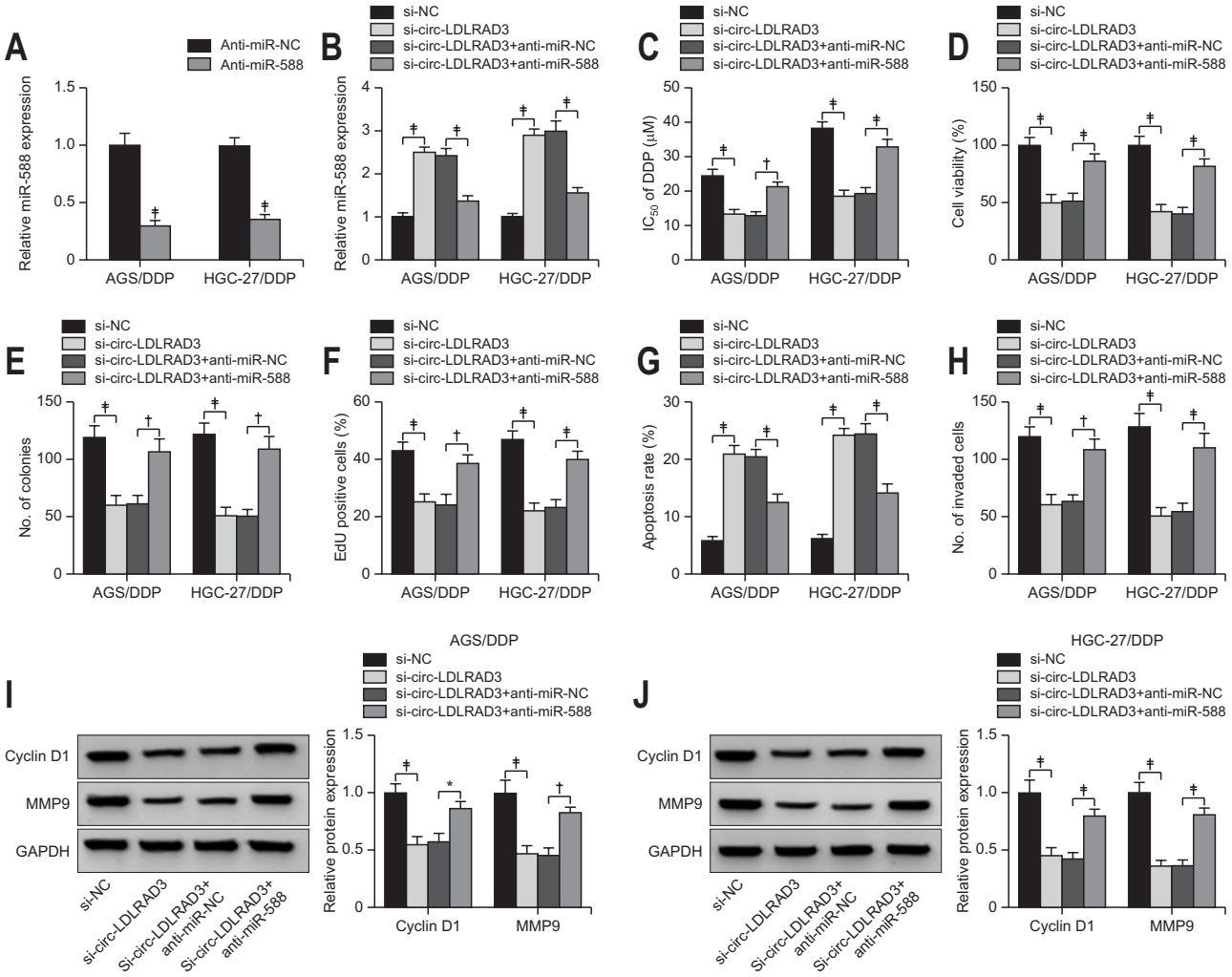

Fig. 4. circ-LDLRAD3 exerts its functions by targeting miR-588. (A) The efficiency of anti-miR-588 was assessed by qPCR. In AGS/DDP and HGC-27/DDP cells transfected with si-circ-LDLRAD3 or si-circ-LDLRAD3+anti-miR-588, (B) the expression of miR-588 was detected by qPCR. (C, D) The IC_{50} of DDP and cell viability were detected by CCK-8 assay. (E, F) Colony formation and EdU assays were performed to assess cell proliferation. (G) Flow cytometry assays were used to assess cell apoptosis. (H) Transwell assays were conducted to assess cell invasion. (I, J) The protein levels of cyclin D1 and MMP9 were detected by Western blotting.
circ-LDLRAD3, hsa_circ_0006988; qPCR, quantitative real-time polymerase chain reaction; DDP, cisplatin; NC, negative control; IC_{50}, half maximal inhibitory concentration. *p<0.01, †p<0.001, ‡p<0.0001.

5. miR-588 inhibited SOX5 expression by binding to SOX5 3'UTR

Public bioinformatics database showed that miR-588 is bound to SOX5 3'UTR via several binding sites (Fig. 5A). The cotransfection of miR-588 and WT-SOX5 3'UTR notably decreased luciferase activity, confirming the binding between miR-588 and SOX5 3'UTR (Fig. 5B and C). The expression of SOX5 mRNA was notably enhanced in DDP-resistant tumor tissues compared to DDP-sensitive tumor tissues (Fig. 5D), and SOX5 mRNA expression was nega-

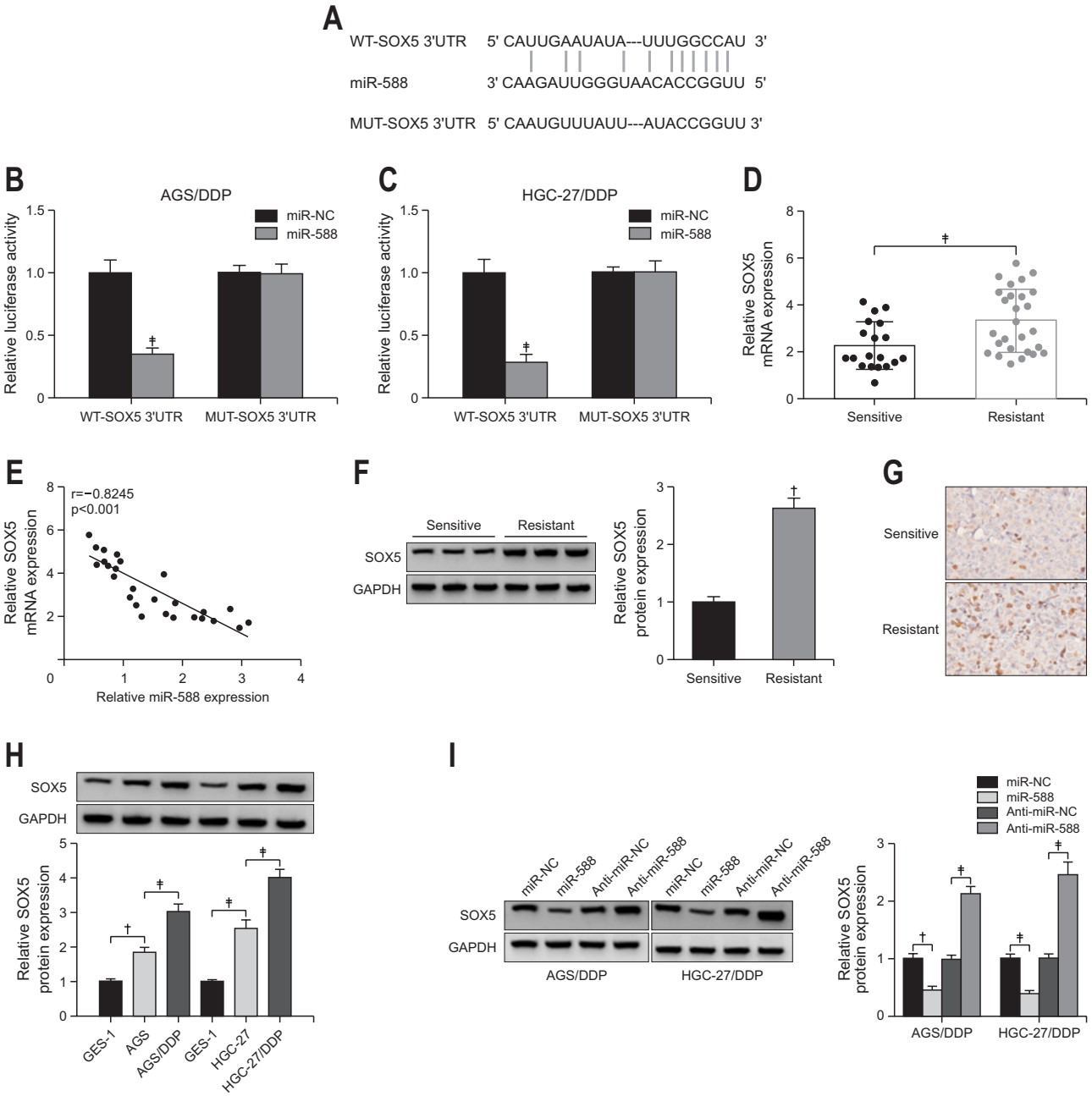

Fig. 5. SOX5 is a target of miR-588. (A) The WT and MUT sequences of SOX5 3'UTR are shown. (B, C) The binding relationship between miR-588 and SOX5 3'UTR was confirmed by dual-luciferase reporter assay. (D) The expression of SOX5 mRNA in DDP-sensitive/resistant tumor tissues was detected by qPCR. (E) The correlation between SOX5 mRNA expression and miR-588 expression in DDP-resistant tumor tissues. (F) The expression of SOX5 protein in DDP-resistant/sensitive tumor tissues was detected by Western blotting. (G) The abundance of SOX5 in tumor tissues was detected by immunohistochemistry assay (40×). (H) The expression of SOX5 protein in AGS/DDP, HGC-27/DDP and their parental cells was detected by Western blotting. (I) The expression of SOX5 protein in AGS/DDP and HGC-27/DDP cells with miR-588 restoration or inhibition was detected by Western blotting.

SOX5, SRY-box transcription factor 5; WT, wild-type; MUT, mutant; 3'UTR, 3' untranslated region; DDP, cisplatin; NC, negative control; qPCR, quantitative real-time polymerase chain reaction. *p<0.01, †p<0.001, ‡p<0.0001.

tively correlated with miR-588 expression in DDP-resistant tumor tissues (Fig. 5E). Moreover, the high abundance of SOX5 in DDP-resistant tumor tissues was verified by Western blot and IHC assays (Fig. 5F and G). The expression of SOX5 protein was also increased in AGS/DDP and HGC-27/DDP cells compared with that in AGS and HGC-27 cells (Fig. 5H). Additionally, the expression of SOX5 protein was decreased in AGS/DDP and HGC-27/DDP cells with miR-588 enrichment but largely strengthened in cells with miR-588 downregulation (Fig. 5I). The data indicated that SOX5 was a target of miR-588.

6. miR-588 restoration inhibited DDP resistance and cell malignant behaviors in DDP-resistant GC cells by depleting SOX5

The expression of SOX5 was notably increased in AGS/DDP and HGC-27/DDP cells transfected with SOX5 (Fig. 6A). Besides, the expression of SOX5 was declined in AGS/DDP and HGC-27/DDP cells transfected with miR-588 alone but recovered in cells transfected with miR-588+SOX5 (Fig. 6B). The IC_{50} of DDP was declined in AGS/DDP and HGC-27/DDP cells with miR-588 restoration, while the IC_{50} of DDP was partly reinforced in cells with SOX5 reintroduction (Fig. 6C). Through CCK-8 assay, colony formation assay and EdU assay, we believed that the ability of AGS/DDP and HGC-27/DDP cell proliferation was suppressed by miR-588 restoration but recovered by

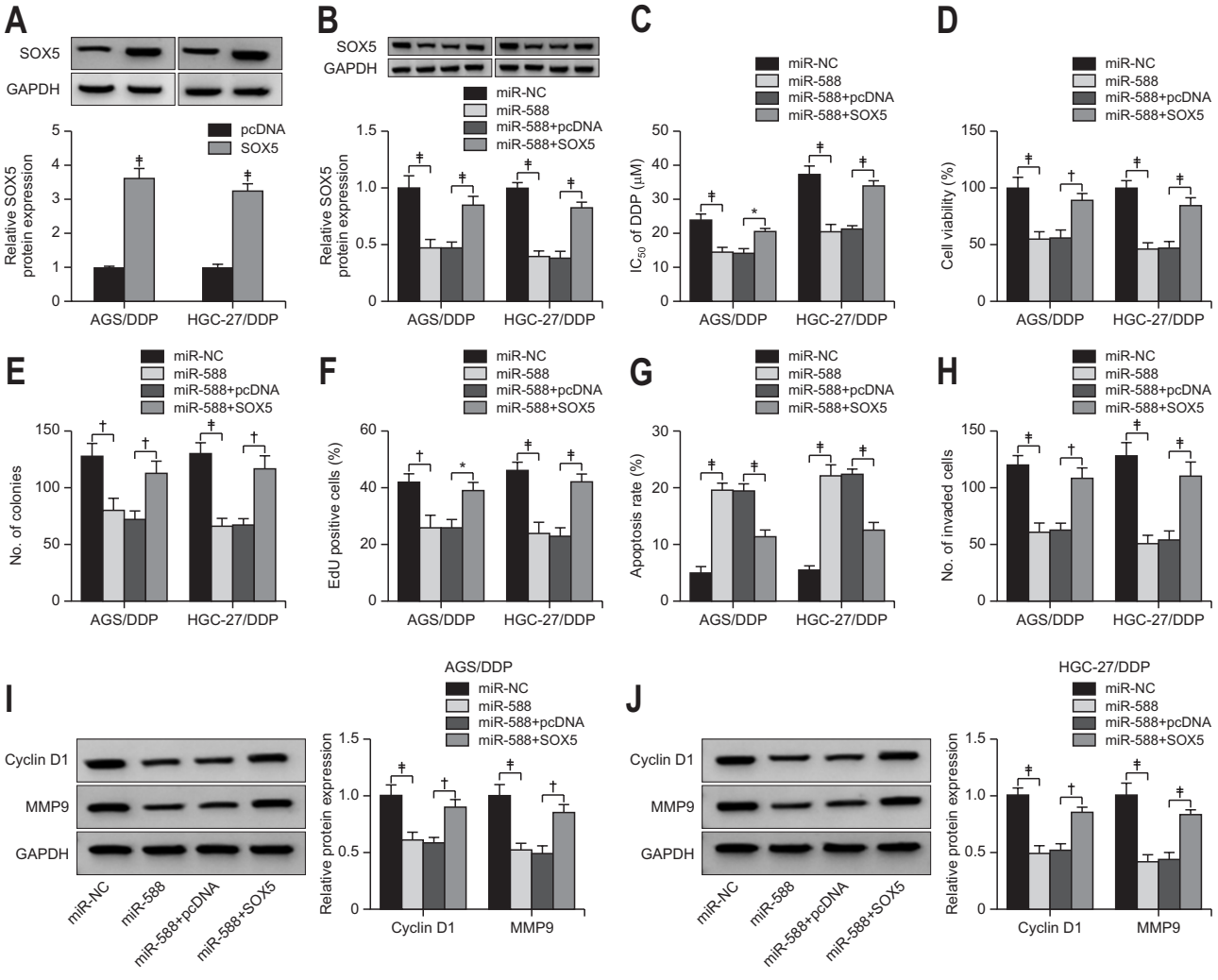

Fig. 6. miR-588 exerts its functions by inhibiting SOX5. (A) The efficiency of SOX5 overexpression was assessed by Western blotting. In AGS/DDP and HGC-27/DDP cells transfected with miR-588 or miR-588+SOX5, (B) the expression of SOX5 protein was detected by Western blotting. (C, D) The IC_{50} of DDP and cell viability were measured by CCK-8 assay. (E, F) Colony formation and EdU assays were performed to assess cell proliferation. (G) Cell apoptosis was determined by flow cytometry assay. (H) Cell invasion was detected by Transwell assay. (I, J) The protein levels of cyclin D1 and MMP9 were detected by Western blotting.
SOX5, SRY-box transcription factor 5; DDP, cisplatin; NC, negative control; IC_{50}, half maximal inhibitory concentration. *p<0.01, †p<0.001, ‡p<0.0001.

the reintroduction of SOX5 (Fig. 6D-F). Besides, miR-588 restoration-induced cell apoptosis was partially blocked by SOX5 overexpression (Fig. 6G). The capacity of cell invasion was suppressed by miR-588 restoration but largely recovered by SOX5 reintroduction (Fig. 6H). In addition, the protein levels of cyclin D1 and MMP9 were reduced in AGS/DDP and HGC-27/DDP cells transfected with miR-588 alone but restored in cells transfected with miR-588+SOX5 (Fig. 6I and J). The data revealed that miR-588 restoration inhibited DDP resistance and cell malignant behaviors in DDP-resistant GC cells by depleting SOX5.

7. SOX5 expression was depleted by circ-LDLRAD3 knockdown but recovered by miR-588 inhibition

Additional study found that the expression of SOX5 mRNA and protein was remarkably declined in AGS/DDP and HGC-27/DDP cells transfected with si-circ-LDLRAD3, while the expression of SOX5 was partially recovered in cells transfected with si-circ-LDLRAD3+anti-miR-588 (Fig. 7). The data suggested that circ-LDLRAD3 knockdown suppressed SOX5 expression by enriching miR-588.

8. circ-LDLRAD3 downregulation inhibited DDP resistance *in vivo*

To determine the role of circ-LDLRAD3 on DDP resistance *in vivo*, xenograft models were constructed. As shown in Fig. 8A and B, DDP administration significantly inhibited tumor volume and tumor weight, and additional circ-LDLRAD3 knockdown inhibited tumor chemoresistance to DDP and further suppressed tumor volume and tumor weight. Besides, the expression of circ-LDLRAD3 and SOX5 protein was decreased, while the expression of miR-588 was enhanced in tumor tissues from the sh-circ-LDLRAD3-administered groups (Fig. 8C and D), hinting that the inhibitory tumor growth was associated with the decreased expression of circ-LDLRAD3 and SOX5, and the enhanced expression of miR-588. IHC assay showed that the abundance of SOX5 and Ki67 was decreased in the sh-circ-LDLRAD3+PBS group compared to sh-NC+PBS group, and their abundance was also decreased in the sh-circ-LDLRAD3+DDP group compared to sh-NC+DDP group (Fig. 8E), suggesting that circ-LDLRAD3 downregulation inhibited tumor growth.

9. circ-LDLRAD3 could be transferred by exosomes and was overexpressed in exosomes deriving from AGS/DDP and HGC-27/DDP cells

Exosomes were isolated from AGS/DDP and HGC-27/DDP cells. The morphology of exosomes was identified by transmission electron microscopy, and a typical lipid

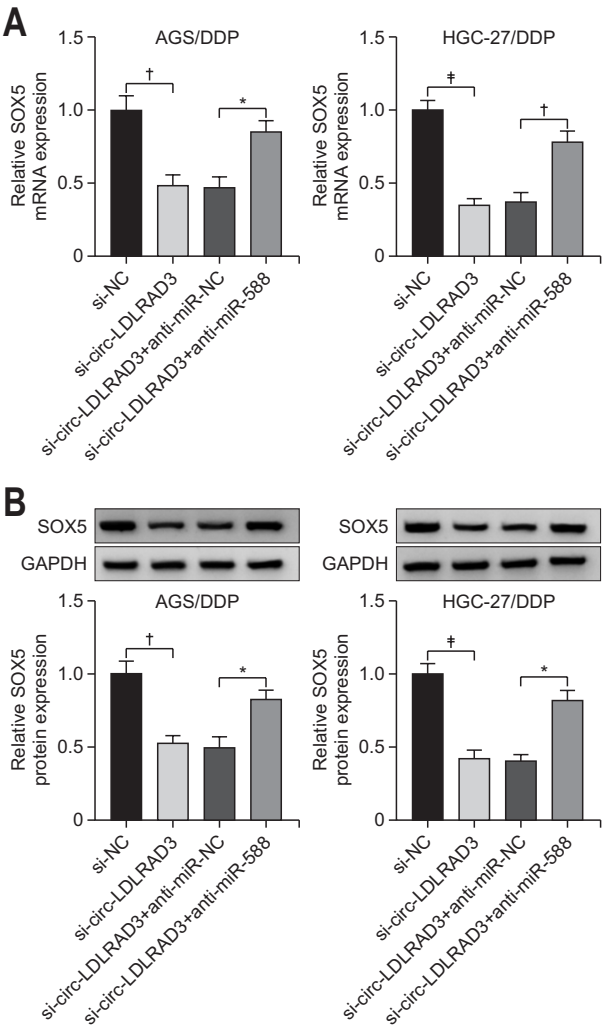

Fig. 7. circ-LDLRAD3 knockdown inhibited the expression of SOX5 by enriching miR-588. (A, B) The expression of SOX5 mRNA and protein in AGS/DDP and HGC-27 cells transfected with si-circ-LDLRAD3 alone or si-circ-LDLRAD3+anti-miR-588 was detected by qPCR and Western blotting.
circ-LDLRAD3, hsa_circ_0006988; SOX5, SRY-box transcription factor 5; qPCR, quantitative real-time polymerase chain reaction; DDP, cisplatin; NC, negative control. *p<0.01, †p<0.001, ‡p<0.0001.

bilayer membrane structure was observed in exosomes isolated from AGS/DDP and HGC-27/DDP cells (Fig. 9A). The markers of exosomes, including CD63 and CD9, were noticeably detected in cell exosomes by Western blot but rarely detected in supernatant (Fig. 9B). The data verified the existence of exosomes. In addition, we found that the expression of circ-LDLRAD3 was higher in exosomes isolated from AGS and HGC-27 cells compared to GES-1 cells, and circ-LDLRAD3 expression was higher in exosomes isolated from AGS/DDP and HGC-27/DDP cells compared to AGS and HGC-27 cells (Fig. 9C). Exosomes isolated from AGS/DDP and HGC-27/DDP cells were used to incubate AGS and HGC-27 cells, respectively, and we

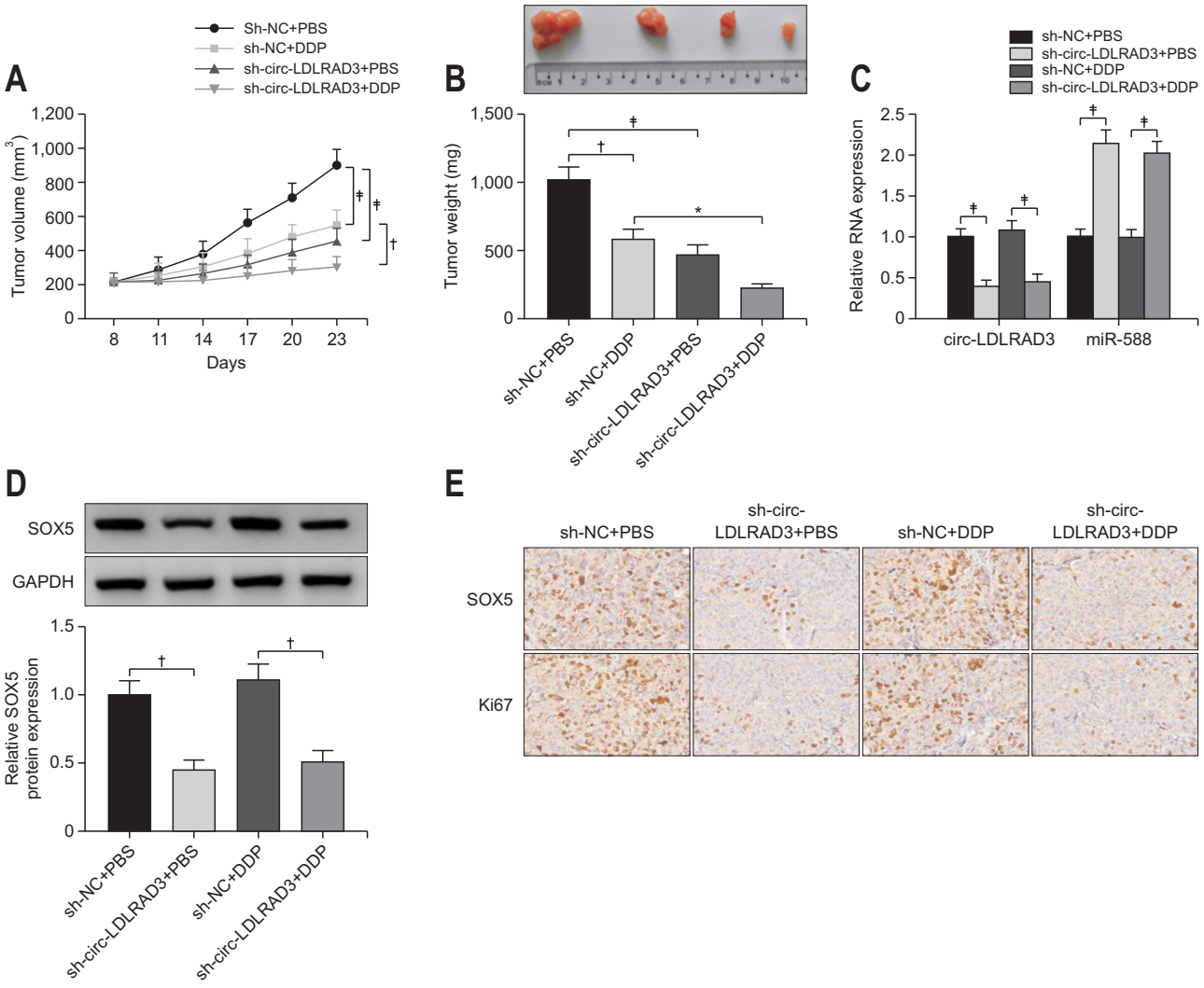

Fig. 8. circ-LDLRAD3 knockdown suppressed tumor growth *in vivo*. (A) During the period of tumor growth, tumor volume was measured every 3 days. (B) Tumor weight was measured after tissue excision. (C) The expression of circ-LDLRAD3 and miR-588 in tumor tissues was detected by qPCR. (D) The expression of SOX5 protein in tumor tissues was measured by Western blotting. (E) The abundance of SOX5 and Ki67 in tumor tissues was monitored by immunohistochemistry assay (40×).
circ-LDLRAD3, hsa_circ_0006988; qPCR, quantitative real-time polymerase chain reaction; SOX5, SRY-box transcription factor 5; PBS, phosphate-buffered saline; DDP, cisplatin; NC, negative control. *p<0.01, †p<0.001, ‡p<0.0001.

found that the expression of circ-LDLRAD3 was strikingly elevated in AGS and HGC-27 cells after exosomes incubation (Fig. 9D). Moreover, the expression of circ-LDLRAD3 was notably declined in exosomes isolated from AGS/DDP and HGC-27/DDP cells with the treatment of GW4869 (an inhibitor of exosomes) (Fig. 9E). These data suggested that circ-LDLRAD3 could be transferred by exosomes and was overexpressed in exosomes deriving from AGS/DDP and HGC-27/DDP cells.

DISCUSSION

circRNA has gradually become a hotspot in the field of RNA and cancer research, whereas the functions of most circRNAs have not been discovered yet. In this study, we focused on circ-LDLRAD3 and discovered that a higher expression level of circ-LDLRAD3 was shown in DDP-resistant GC tissues and cells. The downregulation of circ-LDLRAD3 enhanced DDP sensitivity in DDP-resistant GC cells and inhibited cell proliferation, survival and invasion. For mechanism analysis, we found that circ-LDLRAD3 could serve as miR-588 sponge to releasing SOX5, meaning that circ-LDLRAD3 knockdown blocked the development of DDP-resistant GC through miR-588 enrichment-mediated SOX5 inhibition. Besides, circ-LDLRAD3 was shown to be highly expressed in exosomes from DDP-resistant cells, which provides a basis for circ-LDLRAD3 as

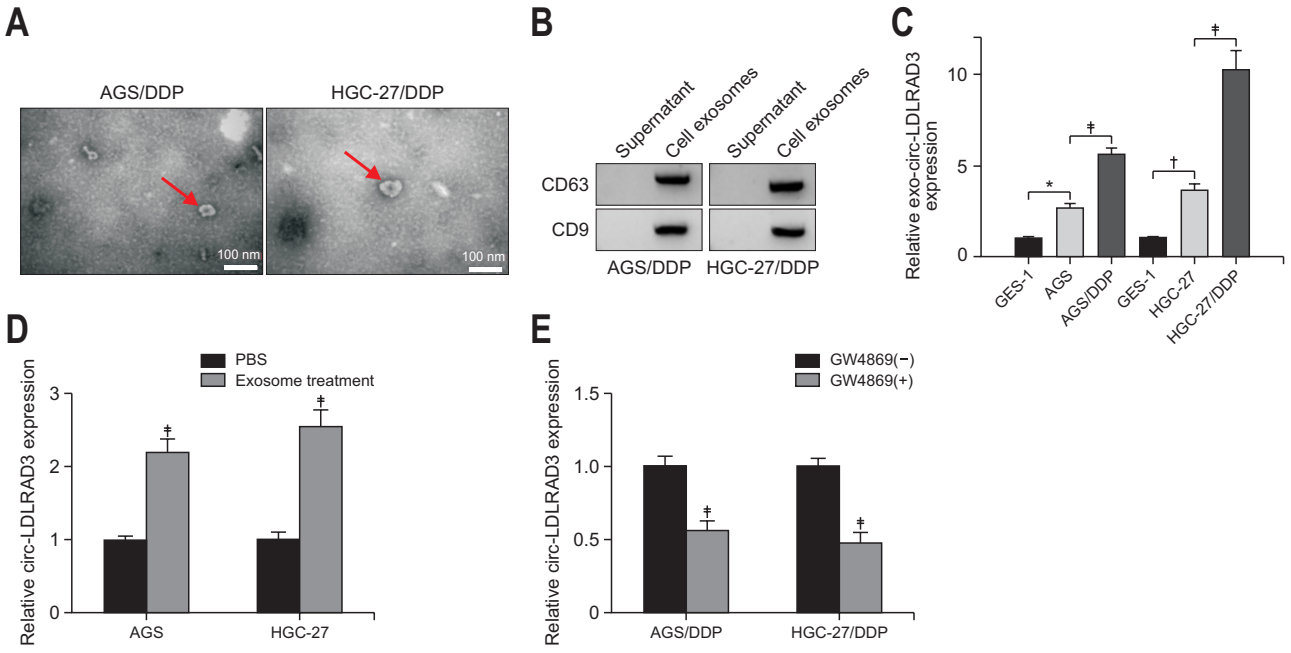

Fig. 9. circ-LDLRAD3 was highly expressed in exosomes isolated from DDP-resistant gastric cancer cells. (A) The morphology of the isolated exosomes were identified by transmission electron microscopy. (B) The expression of exosomes-related proteins was detected by Western blotting. (C) The expression of circ-LDLRAD3 in exosomes isolated from various cells was detected by qPCR. (D) Exosomes isolated from AGS/DDP and HGC-27 cells were used to incubate AGS and HGC-27 cells, and the expression of circ-LDLRAD3 was measured by qPCR. (E) The expression of circ-LDLRAD3 in exosomes treated with exosomes inhibitor was detected by qPCR.
circ-LDLRAD3, hsa_circ_0006988; DDP, cisplatin; qPCR, quantitative real-time polymerase chain reaction. *p<0.01, †p<0.001, ‡p<0.0001.

an exosomal biomarker to predict DDP resistance in GC.

circ-LDLRAD3 is derived from the exon5 region of LDLRAD3 mRNA by "back-splicing," with 346 nucleotides in length. circ-LDLRAD3 was previously shown to be upregulated in pancreatic cancer cells, tissues and plasmas, and high circ-LDLRAD3 expression was associated with cancer metastasis and invasion.[15] The knockdown of circ-LDLRAD3 inhibited pancreatic cancer cell proliferation, migration and invasion.[16] The similar effects of circ-LDLRAD3 knockdown were also observed in non-small cell lung cancer, and the data presented that circ-LDLRAD3 knockdown suppressed non-small cell lung cancer cell proliferation and invasion.[17] A recent study reported the role of circ-LDLRAD3 in GC and mentioned that circ-LDLRAD3 knockdown repressed GC cell proliferation, invasion and migration.[18] Largely consistent with these studies, our study discovered that circ-LDLRAD3 expression was higher in cancer tissues and cells relative to normal tissues and non-cancer cells, and circ-LDLRAD3 expression was further increased in DDP-resistant cancer tissues and cells compared to DDP-sensitive tissues and cells. We assumed that circ-LDLRAD3 high expression was linked to DDP resistance and found that circ-LDLRAD3 knockdown weakened IC_{50} of DDP in DDP-resistant GC cells and inhibited cell proliferation, survival and invasion. All findings indicated that circ-LDLRAD3 drove the development of DDP chemoresistance in GC. Moreover, we found that circ-LDLRAD3 expression was notably enhanced in exosomes from DDP-resistant GC cells compared to normal GC cells, suggesting that circ-LDLRAD3 could be transported by exosomes. It has been demonstrated that cancer-derived exosomes play effects on the development of cancers and are widely distributed in numerous body fluids.[19] CircRNAs carried by exosomes are regarded as diagnostic, prognostic or predictive biomarkers in cancers.[19,20] We thus speculated that exosomal circ-LDLRAD3 might be used as a biomarker to predict DDP resistance in GC, which needed further exploration.

Bioinformatics tools showed that there were binding sites of miR-588 on circ-LDLRAD3. To determine whether circ-LDLRAD3 played functions by acting as miR-588 sponge, we performed rescue experiments and found that the inhibitory IC_{50} of DDP, cell proliferation, survival and invasion by circ-LDLRAD3 knockdown were partially recovered by miR-588 depletion. Previous studies reported that miR-588 was downregulated in GC, and miR-588 overexpression inhibited GC cell migration, invasion and epithelial-mesenchymal transition.[12,21] Besides, the tumor suppressor role of miR-588 was also determined in breast cancer and osteosarcoma.[22,23] Similarly, our data manifested that miR-588 restoration inhibited IC_{50} of DDP, cell proliferation, survival and invasion in DDP-resistant GC

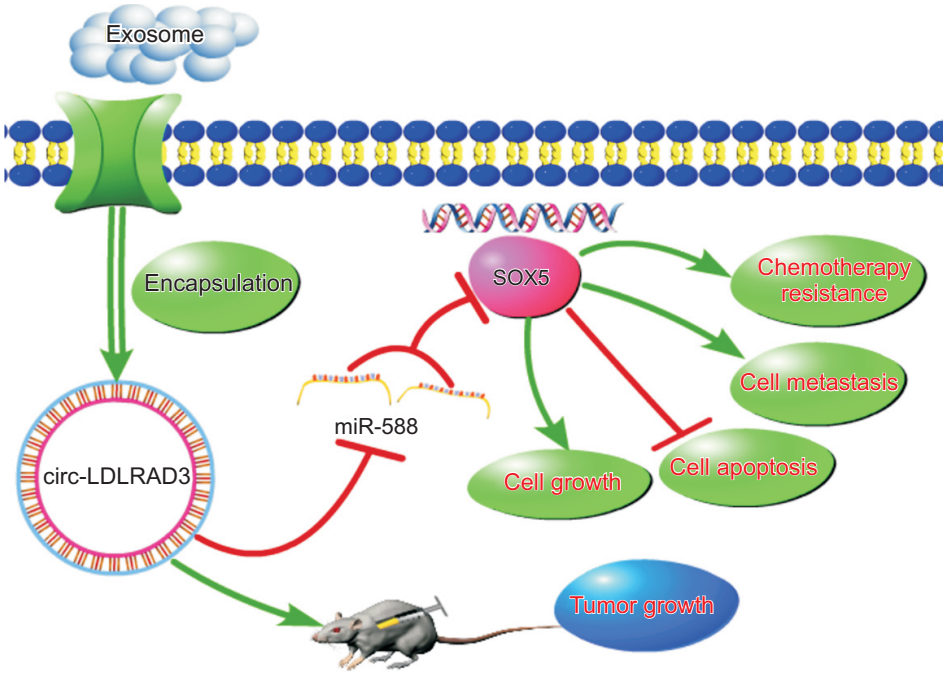

Fig. 10. Graphic summary illustrating the main findings of the present study.
circ-LDLRAD3, hsa_circ_0006988; SOX5, SRY-box transcription factor 5.

cells, hinting that the enrichment of miR-588 might be a strategy against DDP resistance in GC treatment.

Furthermore, bioinformatics tools provided binding sites of miR-588 on SOX5 3'UTR. Besides, SOX5 expression was negatively correlated with miR-588 expression in DDP-resistant tumor tissues. SOX5 was previously reported to promote GC cell migration and invasion by activating epithelial-mesenchymal transition, and high SOX5 expression was linked to clinical metastasis and poor prognosis of GC patients.[13] SOX5 expression was regulated by miR-539, and miR-539 suppressed GC cell proliferation and migration by depleting SOX5.[24] Considering the vital role of SOX5 in GC, we screened SOX5 as a target of miR-588 in our study. Rescue experiments showed that SOX5 overexpression recovered DDP resistance, cell proliferation, survival and invasion that were inhibited by miR-588 restoration, indicating that miR-588 inhibited the development of DDP-resistant GC by sequestering SOX5.

In conclusion, circ-LDLRAD3 knockdown enhanced DDP chemosensitivity and inhibited the malignant development in DDP-resistant GC through miR-588-mediated SOX5 inhibition (Fig. 10). Exosomal circ-LDLRAD3 might be a promising biomarker for the detection of DDP-resistant GC. This study further disclosed the role of circ-LDLRAD3 in GC, and targeting circ-LDLRAD3 might be a new strategy for GC treatment.

CONFLICTS OF INTEREST

No potential conflict of interest relevant to this article was reported.

ACKNOWLEDGEMENTS

This work was supported by Medical science and technology research plan of Henan Province in 2020 (Key projects jointly built by provinces and ministries) (grant number: SBGJ202002128).

AUTHOR CONTRIBUTIONS

Conceptualization and methodology: F.C., L.Z. Formal analysis and data curation: Y.J., L.L., H.W. Validation and investigation: Q.L., F.C. Writing - original draft preparation: Q.L., F.C., L.Z., Y.J. Writing - review and editing: Q.L., F.C., L.Z., Y.J. Approval of final manuscript: all authors.

ORCID

Qianping Liang https://orcid.org/0000-0003-0507-2954
Feifei Chu https://orcid.org/0000-0001-5689-4136
Lei Zhang https://orcid.org/0000-0002-7709-8902
Yuanyuan Jiang https://orcid.org/0000-0002-7438-4081
Lu Li https://orcid.org/0000-0002-3880-0500

Huili Wu https://orcid.org/0000-0002-9678-4596

REFERENCES

1. Bray F, Ferlay J, Soerjomataram I, Siegel RL, Torre LA, Jemal A. Global cancer statistics 2018: GLOBOCAN estimates of incidence and mortality worldwide for 36 cancers in 185 countries. CA Cancer J Clin 2018;68:394-424.
2. Li Z, Lü M, Zhou Y, et al. Role of long non-coding RNAs in the chemoresistance of gastric cancer: a systematic review. Onco Targets Ther 2021;14:503-518.
3. Wagner AD, Unverzagt S, Grothe W, et al. Chemotherapy for advanced gastric cancer. Cochrane Database Syst Rev 2010;(3):CD004064.
4. Hong L, Han Y, Yang J, et al. MicroRNAs in gastrointestinal cancer: prognostic significance and potential role in chemoresistance. Expert Opin Biol Ther 2014;14:1103-1111.
5. Braicu C, Zimta AA, Gulei D, Olariu A, Berindan-Neagoe I. Comprehensive analysis of circular RNAs in pathological states: biogenesis, cellular regulation, and therapeutic relevance. Cell Mol Life Sci 2019;76:1559-1577.
6. Fang X, Wen J, Sun M, Yuan Y, Xu Q. CircRNAs and its relationship with gastric cancer. J Cancer 2019;10:6105-6113.
7. Cui C, Yang J, Li X, Liu D, Fu L, Wang X. Functions and mechanisms of circular RNAs in cancer radiotherapy and chemotherapy resistance. Mol Cancer 2020;19:58.
8. Huang X, Li Z, Zhang Q, et al. Circular RNA AKT3 upregulates PIK3R1 to enhance cisplatin resistance in gastric cancer via miR-198 suppression. Mol Cancer 2019;18:71.
9. Harrandah AM, Mora RA, Chan E. Emerging microRNAs in cancer diagnosis, progression, and immune surveillance. Cancer Lett 2018;438:126-132.
10. Panda AC. Circular RNAs act as miRNA sponges. Adv Exp Med Biol 2018;1087:67-79.
11. Lee S, Vasudevan S. Post-transcriptional stimulation of gene expression by microRNAs. Adv Exp Med Biol 2013;768:97-126.
12. Zhou X, Xu M, Guo Y, et al. MicroRNA-588 regulates invasion, migration and epithelial-mesenchymal transition via targeting EIF5A2 pathway in gastric cancer. Cancer Manag Res 2018;10:5187-5197.
13. You J, Zhao Q, Fan X, Wang J. SOX5 promotes cell invasion and metastasis via activation of Twist-mediated epithelial-mesenchymal transition in gastric cancer. Onco Targets Ther 2019;12:2465-2476.
14. Fang QL, Li KC, Wang L, Gu XL, Song RJ, Lu S. Targeted inhibition of CCL22 by miR-130a-5p can enhance the sensitivity of cisplatin-resistant gastric cancer cells to chemotherapy. Cancer Manag Res 2020;12:3865-3875.
15. Yang F, Liu DY, Guo JT, et al. Circular RNA circ-LDLRAD3 as a biomarker in diagnosis of pancreatic cancer. World J Gastroenterol 2017;23:8345-8354.
16. Yao J, Zhang C, Chen Y, Gao S. Downregulation of circular RNA circ-LDLRAD3 suppresses pancreatic cancer progression through miR-137-3p/PTN axis. Life Sci 2019;239:116871.
17. Xue M, Hong W, Jiang J, Zhao F, Gao X. Circular RNA circ-LDLRAD3 serves as an oncogene to promote non-small cell lung cancer progression by upregulating SLC1A5 through sponging miR-137. RNA Biol 2020;17:1811-1822.
18. Wang Y, Yin H, Chen X. Circ-LDLRAD3 enhances cell growth, migration, and invasion and inhibits apoptosis by regulating miR-224-5p/NRP2 axis in gastric cancer. Dig Dis Sci 2021;66:3862-3871.
19. Kok VC, Yu CC. Cancer-derived exosomes: their role in cancer biology and biomarker development. Int J Nanomedicine 2020;15:8019-8036.
20. Jalalian SH, Ramezani M, Jalalian SA, Abnous K, Taghdisi SM. Exosomes, new biomarkers in early cancer detection. Anal Biochem 2019;571:1-13.
21. Chen Y, Zhang J, Gong W, Dai W, Xu X, Xu S. miR-588 is a prognostic marker in gastric cancer. Aging (Albany NY) 2020;13:2101-2117.
22. Yu M, Zhang X, Li H, Zhang P, Dong W. MicroRNA-588 is downregulated and may have prognostic and functional roles in human breast cancer. Med Sci Monit 2017;23:5690-5696.
23. Liu R, Ju C, Zhang F, et al. LncRNA GSEC promotes the proliferation, migration and invasion by sponging miR-588/EIF5A2 axis in osteosarcoma. Biochem Biophys Res Commun 2020;532:300-307.
24. Ding S, Zhang Y. MicroRNA-539 inhibits the proliferation and migration of gastric cancer cells by targeting SRY-box 5 gene. Mol Med Rep 2019;20:2533-2540.